Dynamics of the Transport of Ionic and Atomic Cesium in RF-driven Ion Sources for ITER NBI

R. Gutser, D. Wünderlich, U. Fantz, and the N-NBI Team

Max-Planck-Institut für Plasmaphysik, Euratom Association, D-85748 Garching, Germany

E-mail: raphael.gutser@ipp.mpg.de

Abstract. The neutral beam injection heating system of the future ITER fusion experiment will rely on the acceleration and neutralization of negative hydrogen ions. Cesium seeding into negative ion sources is a prerequisite to obtain the required ion current at a maximum pressure of 0.3 Pa and a tolerable level of co-extracted electrons. Both the stability and the delivered current density of the ion source depend highly on the cesium conditions of the production surface during plasma and vacuum phases. The Monte Carlo code CsFlow3D was developed and applied to simulate the distribution and time dynamics of neutral and ionic cesium during long pulses of the IPP prototype RF-driven ion source. These transient simulations show that the release of cesium accumulated within the ion source during the operation phase is the dominant mechanism to obtain cesium flux onto the production surface for negative ions (plasma grid). Studies of the spatial distribution of the deposits and the corresponding time dynamics and cesium flux profile are presented during long pulses. These show that the cesium flux onto the plasma grid has a high time variation which is a consequence of the transient release of reservoirs. While a high ionic flux is generated within the first seconds of the discharge, a broad neutral-dominated flux peak evolves during the total pulse interval.

1. Introduction

The injection of fast neutral particles into a magnetically-confined fusion plasma depositing energy by collision processes is an important method for plasma heating and current drive.

Two high performance neutral beam injection (NBI) systems which deliver 1 MeV D^0 neutral beams with a power of 16.7 MW [1] are required for heating and current drive in the next generation fusion experiment ITER. These systems are based on the acceleration and neutralization of a high-energy ion beam within a gas target. While the neutralization efficiency for systems based on positive hydrogen ions tends to zero for energies above several 100 keV, the neutralization efficiency of negative H/D ions is still 60 % for the required energy [2]. Hence, the neutral beam heating system for ITER will be based on negative ions (N-NBI).

Special requirements have to be fulfilled by a negative H/D ion source for ITER. Each

ion source must deliver a total D^- current of 40 A for a pulse length of 3600 sec at a pressure of 0.3 Pa while maintaining an electron to ion ratio < 1 [1][3].
For the mentioned ITER operation requirements, typical $D^-(H^-)$ ion current densities of $j = 200(300)$ A/m^2 have been achieved from negative ion sources up to now[4]. To meet the required current of 40 A, the effective extraction area needs to be 2000 cm^2. This is significantly larger than the extraction area of several cm^2 used in today's small negative hydrogen ion sources for particle accelerators. For large dimensions of several thousand cm^2, the homogeneity of the extracted ion current density is an important factor for the accelerated beam. An inhomogeneous current density creates also a variation of the ion optics across the beam area resulting in an improper beam focus. Thus, the ion source for ITER N-NBI will require an inhomogeneity lower than 10%.
A high-performance, large-area RF-driven negative hydrogen ion source for the ITER neutral beam injection systems is being developed at IPP [4]. The test beds for the RF-driven ion source prototype are operated with D_2 and H_2. As a consequence of the production of neutrons in case of deuterium operation, hydrogen is more often used because of the advantage in safety aspects.
The significant benefit by the use of an external RF-coil is its essentially maintenance-free source operation which is beneficial to fulfill the remote handling requirement of ITER. As a consequence of this development, the ITER committee has decided to adopt the RF-driven ion source as the reference source for the ITER neutral beam injectors [1].
Optimizing the cesium-enhanced surface production is one of the central aspects of research and development in order to meet the ITER requirements. The additional electron of negative hydrogen ions has a low binding energy (0.75 eV) which is beneficial for the neutralization - but this makes the negative ion vulnerable to destruction processes. Hence, the current densities delivered from negative ion sources for N-NBI are significantly lower compared to positive ion sources for NBI (several 1000 A/cm^2). Additionally, electrons are extracted together with the negative ions. These electrons have to be removed at low energies in order to avoid damage to the accelerator system and beamline components.
The physical processes responsible for the generation of negative hydrogen ions are different from the production mechanisms in positive ion sources, where the hydrogen ions can be extracted directly from the source plasma. Negative ion sources require special channels to generate a significant amount of negative ions, which need to be transported to the ion extraction system. The production of negative hydrogen ions takes place either by the attachment of slow electrons in the plasma volume (volume production [5]) or by electron transfer from a low work function converter surface (surface production [6]). Considering the current status of research it is only possible to meet the requirements regarding the (high) negative ion and (low) co-extracted electron currents at the required source pressure (0.3 Pa) by surface production: positive and neutral hydrogen particles which are created by a plasma source are directed onto a converter surface (plasma grid), where they form negative ions by picking up one or

more electrons. This kinetically assisted electron transfer process is strongly influenced by the work function of the surface. The work function of the bare plasma grid surface which is made of molybdenum- or tungsten-coated copper is above 4 eV. In this case only a negligible amount of negative ions is created by surface production [7].
At present, the operation of negative ion sources at ITER-relevant conditions is only possible by covering the plasma grid with an electropositive element like the alkaline metal cesium reducing its work function. Therefore, cesium vapor is introduced into the ion source both during source operation (plasma phases) and in between the plasma pulses (vacuum phases), while keeping the inner source walls at a temperature of 20 to 50 °C and the plasma grid at 150 °C. This choice of temperatures is based on empirical observations of the performance of the ion source.
In theory, a proper cesium coating can reduce the work function of a molybdenum-coated surface under ultra high vacuum conditions to values as low as 1.4 eV [8]. However, recent studies under conditions relevant for negative ion sources [9] show a value around 2 eV. The actual value which is achievable in practical ion applications depends on the specific properties, such as temperature and the degree of contamination by residual gas.
Lowering the work function makes it is possible to obtain an increase of the negative ion production by one order of magnitude while the undesired current of co-extracted electrons drops significantly [4]. Nevertheless, the use of cesium creates a dependence of the source performance on the cesium coverage of the plasma grid. Cesium within ion source forms deposits on the source walls which may be released depending on the specific wall conditions. This process creates a dynamical re-distribution of cesium within the ion source causing a variation of the cesium coverage of the plasma grid in time and space.
The ion source for the ITER N-NBI will be significantly larger than current negative ion sources and the spatial distribution and time stability of the injected cesium within the system becomes the dominant factor for the overall source performance. A numerical model to simulate the transient distribution of cesium is therefore highly important for diagnostics and optimization purposes. The transport code CsFlow3D was developed to model the dynamics and distribution of atomic and ionic cesium within an ion source. Time-resolved cesium flux and accumulation profiles on relevant areas, especially the plasma grid, were obtained by the code both during the vacuum and plasma phases of the ion source. Special care was taken for the gathering of input parameters to ensure that these are relevant for the conditions within the RF-driven ion source and to benchmark them with experimental results from the ion source test facility.

2. The RF-driven Negative Ion Source

A brief description of the RF-driven ion source is given in the following section, while detailed information regarding the individual components and operation parameters are available from [4]. The operation principle of a RF-driven ion source for surface

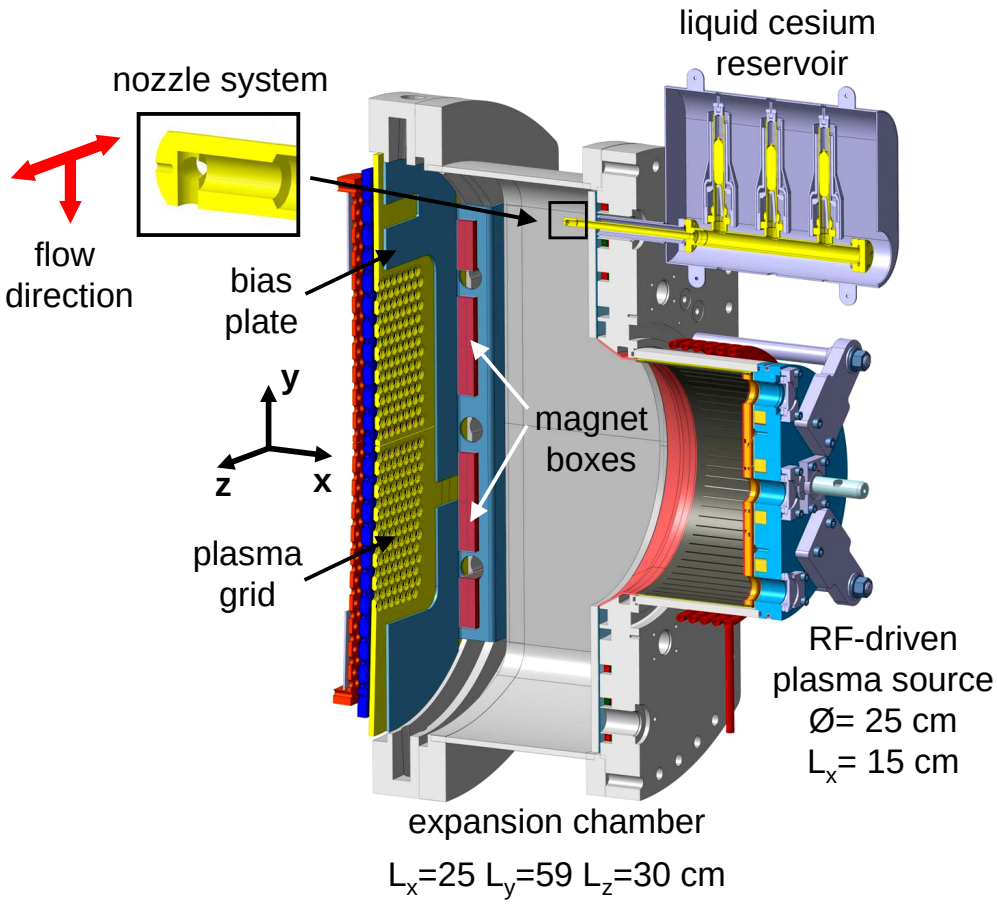

Figure 1. Drawing of the IPP RF-driven ion source prototype attached to the MANITU test facility showing the driver, the expansion chamber and the plasma grid. The liquid-reservoir based cesium injection system is attached to the backplate of the source.

generated negative hydrogen ions relies on the generation of a hydrogen plasma. The flow of plasma particles onto the cesium coated plasma grid surface induces surface conversion. A high voltage extraction system is used to extract the surface generated negative ions.

Figure 1 shows a CAD drawing of the ion source, which is divided into three parts: driver, expansion region and extraction region. A low pressure and low temperature hydrogen plasma is generated by inductive coupling by a 1 MHz RF coil at a driver pressure of 0.3 Pa. A typical RF power of 100 kW is available for plasma generation. A temporary gas puff together with an electron emitting ThO_2-coated tungsten starter filament at the backside of the driver ensures a reliable plasma start-up.

The H_2, H, H^+, H_2^+ and e^- particles formed in the driver enter the expansion region. The electrons initially generated in the driver have a high density and also temperature compared to the binding energy of negative ions (see figure 2). This causes a high probability for destructive collisions with H^- which can detach the additional electron.

An electron cooling mechanism is therefore a prerequisite to reduce the rate of electron detachment near the production surface. Therefore, permanent magnet boxes at the source periphery (see magnet boxes in figure 1) are used to create a magnetic filter field with a strength of approximately 7 mT (hydrogen operation) at the center of the expansion region. A higher filter field is required for source operation with deuterium. Typically, an electron temperature below 2 eV and an electron density within the range of 10^{17} m^{-3} are obtained near the plasma grid converter surface [10][11].
The IPP negative ion source test facilities are operated with pulses of a length shorter than 10 sec up to several 1000 sec. A background vacuum of 10^{-4} Pa is maintained in the plasma-off phases between the plasma pulses. Pulses with a duration of 3600 sec have been achieved at the long-pulse test facility MANITU [12][13].
The dominant generation mechanism in the negative ion source for ITER N-NBI is surface production:

$$H^+ + e^-(\text{wall}) \rightarrow H + e^-(\text{wall}) \rightarrow H^-, \tag{1}$$

$$H + e^-(\text{wall}) \rightarrow H^-. \tag{2}$$

The surface production takes place by the transfer of an electron into the affinity level of atomic hydrogen (0.75 eV). Molecular hydrogen ions are dissociated and Auger neutralized when they approach the surface.
The plasma grid (see: first grid, figure 1) is used as converter for the surface generation process. The grid is kept at a temperature of 150 °C which turned out to be beneficial for the negative ion production [4].
The surface generated negative ions are accelerated back into the plasma volume by the plasma sheath potential and have to be extracted under the influence of charge exchange collisions, the magnetic field and the extraction potential. This sheath potential can be influenced by biasing the plasma grid against the source body. A bias plate at the potential of the source body which is located near the plasma grid (see bias plate in figure 1) is therefore used to enhance the influence of this effect on the extraction region. Additionally, the biasing the plasma grid is a very effective way to reduce the current of co-extracted electrons.
Collisions with the background plasma are able destroy the surface generated negative ions. The transport of negative ions at surface areas close to the driver is strongly reduced by the correspondingly high electron temperature and density. Hence, only negative ions generated on the plasma grid surface are able to contribute significantly to the extracted current density. Negative ions that are able to enter the extraction system through the plasma grid apertures are immediately accelerated by the extraction voltage.
The ion beam formation is accomplished in two stages by a three grid system: the plasma grid, the extraction grid and the grounded grid. In the first step, a voltage of 8 - 10 kV is applied between the plasma and the extraction grid in order to allow the removal of co-extracted electrons at a reasonable power load. This is done by a magnetic deflection field generated by CoSm magnet rods inside the extraction grid structure. A

second voltage of 20 - 30 kV is used for beam acceleration at the IPP ion source test facilities.
The coverage of the plasma grid with the electropositive alkaline metal cesium was found to increase the conversion rate by lowering the work function [14][8] of the plasma grid surface. This coating is generated by the continuous evaporation of elemental cesium from a liquid cesium reservoir into the ion source. A nozzle system which is used to direct the cesium flux is attached to the liquid cesium reservoir at the back flange of the source body. This cesium injection system is shown in figure 1 where the flow directions of the three individual nozzles are emphasized. The total flow of neutral cesium from the reservoir is directed onto both sides ($\pm$z-direction) and the bottom ($-$y-direction) of the expansion chamber in order to obtain an even distribution of the cesium avoiding local concentrations. This nozzle configuration was chosen to reduce coverage of the high voltage grid system. Since the plasma generates a heat load onto the chamber walls, a water cooling system at typical temperatures of 50 °C is used to stabilize the temperature of the ion source chamber walls, which are made from copper.

3. The Cesium Transport Code CsFlow3D

Due to its high vapor pressure, injected cesium is expected to be re-distributed within the ion source chamber creating a dynamical behavior. This dynamical re-distribution is determined by the buildup and depletion of reservoirs on the walls. Hence, it is inadequate to simulate the relevant processes by a steady-state model and the capability of time-resolved computations was a prerequisite for the code development.
The most important requirement for a cesium transport code for the described negative ion source is the computation of the dynamics of cesium transport. This is a consequence of the pressure conditions which alternate by several orders of magnitude between plasma phases (0.3 Pa) and vacuum phases (10^{-4} Pa) changing the characteristics of the cesium flow.
Monte Carlo test particle transport codes are in use to simulate the particle transport for a variety of applications [15][16]. These are based on the computation of large ensembles of independent test particles within a specified particle background for a static electric and magnetic field. The method of independent test particles is applicable for systems, where the interaction between the particles of the transported species can be neglected and is therefore suitable to describe the transport of minority species through a background of field particles. This condition is valid for the transport of neutral and ionic cesium at the parameters of negative ion sources for ITER N-NBI, since the density of ionic and atomic cesium is several orders of magnitude lower than the hydrogen density[11].
A model of the cesium transport in negative ion sources for ITER requires the consideration of the dynamical variation of cesium flow conditions and cesium source terms within the system. The Monte Carlo code CsFlow3D was developed in order to investi-

gate the transient aspects of the cesium transport within the ion source. Geometry and plasma parameters of the IPP prototype negative ion source of the MANITU [4] test facility were implemented in CsFlow3D using a typical extraction area of 204 cm^2.

3.1. Cesium Flow Regimes

Two different flow regimes have to be considered by the model. In the vacuum phases (10^{-4} Pa) between the pulses, the collision path length of atomic cesium is several times larger than the dimensions of the ion source. This means that a free molecular flow regime for atomic cesium is established.
In contrast, the transport of cesium during the discharge phases is affected by collisions with background particles. The alkaline metal cesium has a very low ionization potential of 3.89 eV[17]. Therefore, it is necessary to consider both, atomic and ionic cesium flows at the same time.

3.2. Cesium Transport Equation

The CsFlow3D code is based on the computation of Cs and Cs^+ test particle trajectory ensembles within a background of field particles for densities and temperatures taken from experimental data. The trajectory computation is done by the solution of an ordinary differential equation considering 3D maps of the field and particle data. Further details regarding the particle and field data is given the following sections.
In the vacuum phases, these densities are so low that the cesium test particles follow straight lines until absorption on the walls takes place. Furthermore, no ionization takes place and only neutral cesium has to be considered. In this case the force on the cesium neutrals is zero and the particles follow straight lines.
Considering the plasma phase, collisions with background particles become significant. In case of neutral cesium, the equation consists only of the collision term:

$$m\,\ddot{\vec{r}} = \vec{F}_{\mathrm{Col}}. \tag{3}$$

For cesium ions, the modified Lorentz force equation is used for the transport computation to consider the additional field terms:

$$m\,\ddot{\vec{r}} = q\,(\vec{E} + \vec{v} \times \vec{B}) + \vec{F}_{\mathrm{Col}}, \tag{4}$$

Equation (4) is solved by the combination of time-integration for the Lorentz force term and a Monte Carlo method in order to treat the collision force term $\vec{F}_{\mathrm{Col}}$. The electric $\vec{E}(x, y, z)$ and magnetic field $\vec{B}(x, y, z)$ are determined by a 3D linear interpolation scheme for given field maps.
The transport of cesium is influenced by collisions with the particle background and by the forces from electric and magnetic fields within the ion source. At each time step the particle position and velocity is subject to change due to particle collisions. Additionally, the particle species is subject to change by ionization and recombination.

3.3. Collision Processes

Collision processes of Cs and Cs^+ with H_2, H^+ and e^- species are considered in the calculation. For the sake of simplicity no segmentation of different molecular hydrogen ions was done. Table 1 gives an overview of the included processes and the corresponding dependence of the collision cross section σ on the relative velocity v. A recombination factor of 100% was used in case of the wall recombination processes of Cs^+. While long-

Table 1. Collision processes taken account in CsFlow3D together with the minimum and maximum reaction rate with the source.

Reaction Path	Process	Rates	Source
$Cs^+ + e^-(\text{wall}) \rightarrow Cs$	Wall Recombination		
$Cs^+ + e^- \rightarrow Cs + \hbar\omega$	Radiative Recombination	$\ll 100\ s^{-1}$	[18]
$Cs^+ + H_2 \rightarrow H_2 + Cs^+$	Langevin $\sigma \propto v^{-1}$	$7.4{\cdot}10^4\ s^{-1}$	[19]
$Cs^+ + H^+ \rightarrow H^+ + Cs^+$	Coulomb $\sigma \propto v^{-4}$	2.4 - $2.7{\cdot}10^5\ s^{-1}$	[20]
$Cs + H_2 \rightarrow H_2 + Cs$	Van der Waals $\sigma \propto v^{-\frac{2}{5}}$	$3.3{\cdot}10^5\ s^{-1}$	[21]
$Cs + e^- \rightarrow Cs^+ + 2e^-$	Ionization	$8{\cdot}10^2$ - $4.5{\cdot}10^5\ s^{-1}$	[17]

range Coulomb collisions are taken into account every time step by applying a binary collision model [22], the remaining short-range collisions are treated by the path length estimator algorithm [23], considering an individual probability P_{Col} for each time step:

$$P_{\text{Col}} = 1 - e^{-\Delta t\, \nu_j}, \tag{5}$$

where ν_j is the collision frequency for the individual collision with the species j. The collision frequency is then given by the product of the rate coefficient X_j and the field particle density map $n_j(\vec{r})$:

$$\nu_j = n_j\, X_j. \tag{6}$$

The rate coefficient is obtained by an integration of the product of relative velocity and collision cross section σ_j for a Maxwellian velocity distribution:

$$X_j = < \sigma_j \vec{v} >_{\text{Maxwell},T_j}, \tag{7}$$

where T_j is the particle temperature. The post-collision velocity vector is determined by a binary collision model as described in [22]. An atomic or ionic cesium particle is considered having a specific velocity. The velocity of the collision partner is determined by the Monte Carlo technique using a 3D Maxwell distribution. The equation of momentum and energy conservation of the binary system is solved resulting in a unique post-collision velocity of the cesium particle.

3.4. Particle Data and Field Maps

Ensembles of Cs and Cs^+ test particles are treated for a background of field particle with a given density and Maxwellian temperature distribution. The spatial variation of field

particle parameters is considered by static data maps which are based on measurement at the IPP RF-driven ion source prototype.
Atomic and ionic cesium will undergo elastic collisions with the molecular hydrogen background gas, which is the field-particle species with the highest density within the ion source. A constant molecular hydrogen density of $n_{H_2} = 5\text{x}10^{19}\,\text{m}^{-3}$ with a constant gas temperature of $T_{H_2} = 1200\,K$ during the plasma phase was used for the cesium-transport simulation [11]. These values are within the typical range for the operation conditions of the RF-driven ion source.
An important category of processes for the cesium transport are collisions of cesium neutrals and ions with plasma ions and electrons. As a consequence of the magnetic filter field and the distance between the driver and the extraction region, the plasma parameters undergo a spatial variation within the source. Hence, a decrease of the ion and electron density from the range of $10^{18}\,\text{m}^{-3}$ at the exit of the driver to the mid-range of $10^{17}\,\text{m}^{-3}$ in the expansion region is observed [11]. Furthermore, the electron temperature drops from about $20\,eV$ at the driver exit to values below 2 eV in the extraction region [24].
The CsFlow3D code uses the approximation of a quasi-neutral plasma considering an exponential decay of the plasma density and temperature from the driver to the extraction region using radial-symmetric profiles. The corresponding field particle data maps were developed from probe measurements [24][25][10] applying the Boyd-Twiddy method for the determination of the electron temperature [24]. Figure 2 shows the implemented axial decay profiles of the plasma density and electron temperature and a representative radial profile for x=12 cm.
As described before, 3D maps of the magnetic and electric field are required in order compute the Lorentz force on cesium ions. The complete magnetic field topology of the RF-driven ion source was computed with 3D magnetic field code, developed by D. Ciric [26]. The computed field data was implemented in CsFlow3D. More detailed information regarding the magnetic field configuration of the IPP prototype source are available in [15].
Electric fields are only considered at the extraction apertures while the quasi-neutrality conditions was used for the source plasma assuming a zero electric field in the source plasma. Hence, the positive electric potential of the extraction voltage was modeled by a reflective boundary for cesium ions at the apertures of the plasma grid.

3.5. Cesium Injection and Loss

Cesium injection into the source takes place via evaporation from a temperature controlled liquid reservoir of pure cesium, inserted through the backplate. The total injection rate from the supply for ion source relevant temperature conditions was measured with a surface ionization detector in a special campaign as described in [27]: a cesium injection rate of 10 mg per hour for a typical operation temperature of 150 °C

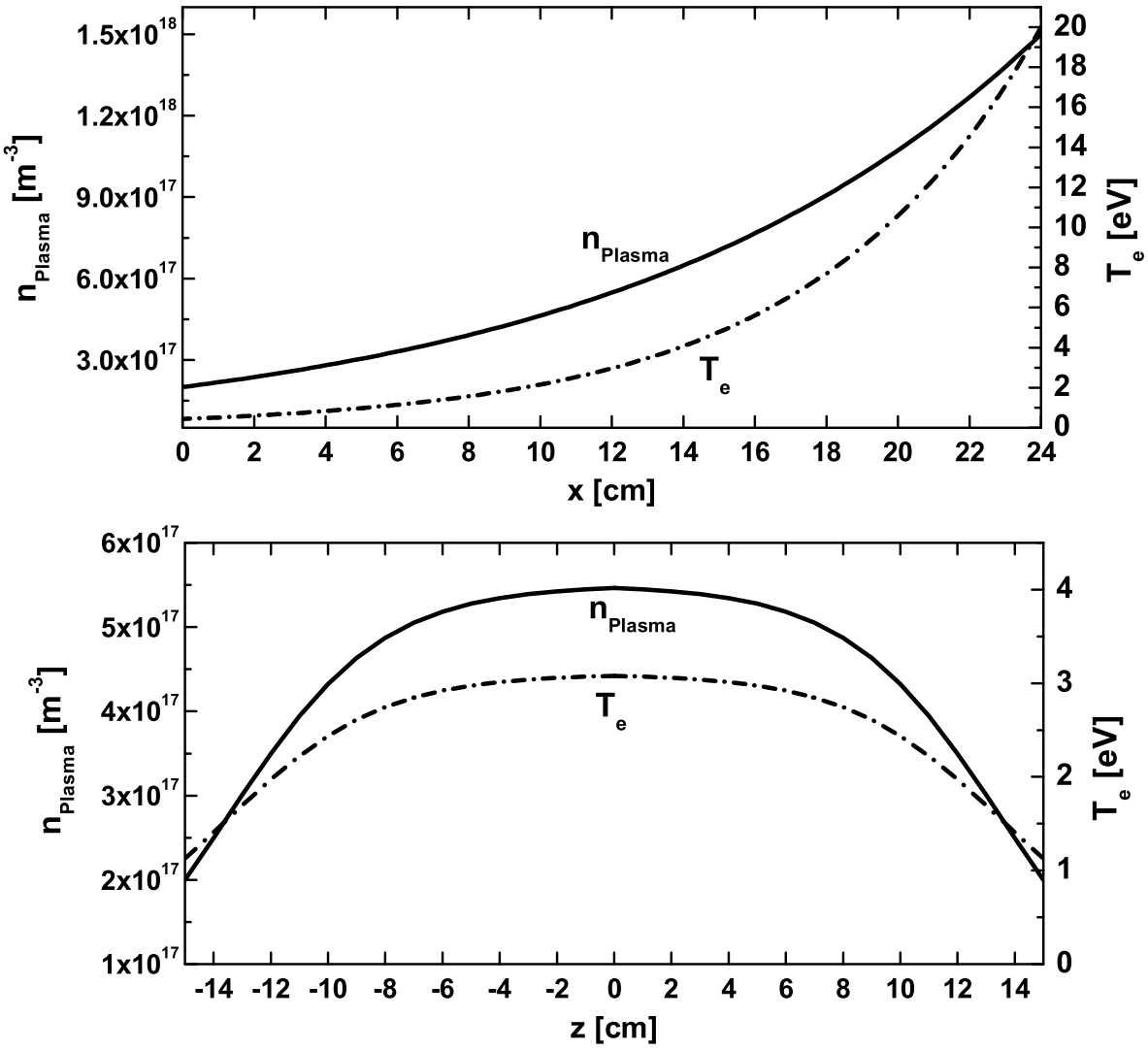

Figure 2. Axial decay profile of the plasma density and electron temperature (top) from the extraction region towards the driver exit and representative radial profile (bottom) for x= 12 cm.

of the supply was obtained.

Besides the total injection rate the profile of the cesium flux from the nozzle system of the evaporation oven was determined in order to compute the cesium distribution within the ion source. The flux profile was computed using a DSMC [28] code considering the geometry and parameters of the nozzle system: the cesium rarefaction flow leaves the supply through three orthogonal nozzles with a diameter of 2.5 mm and a length of 1.5 mm each. Figure 3 shows the angular distribution which was calculated for the IPP nozzle geometry and a cosine distribution representing an ideal orifice for comparison.

Besides the injection, cesium is also lost from the ion source vessel. Atomic cesium is able to leave the ion source through the extraction apertures. During the extraction phase, however, cesium ions are inhibited to leave the source during extraction pulses

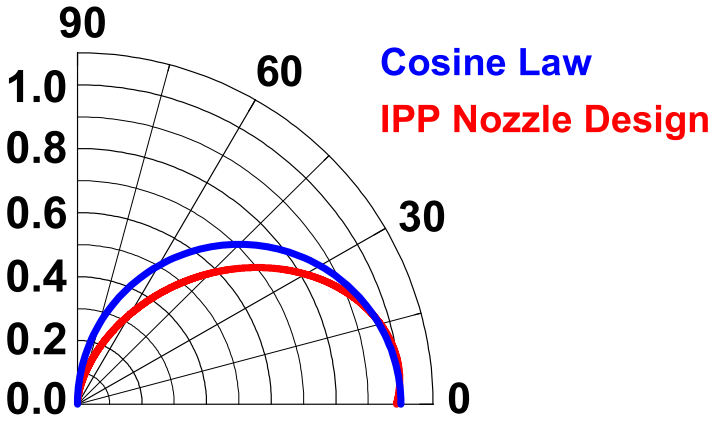

Figure 3. Simulated angular distribution of the flux from a nozzle which is used for the IPP cesium supply and angular distribution of an ideal orifice creating a cosine-type distribution.

as a consequence of the extraction potential of several kV with respect to the source potential.

3.6. Wall Absorption Model

Data and models of the absorption of cesium on metals in literature are limited to ideal monolayer growth at a very low residual gas pressure ($p < 10^{-6}$ Pa) and very clean metal substrates. However, the conditions in the IPP prototype source are very different from an ideal cesium monolayer on mono-crystalline substrates. This is given by the considerably higher residual gas pressure (up to 0.3 Pa during the plasma phase) and contaminations on the walls of the ion source which are not subject to a high temperature treatment. Since cesium reacts instantaneous with impurities on the source walls and the residual gas, this results in the deposition of cesium compounds on the inner surfaces of the source. Figure 4 shows a high contrast photograph of the top wall (y=288 mm) of the (disassembled) ion source after the cesium evaporation of 1000 mg after breaking the vacuum. The black traces on the photograph were identified as cesium oxycuprate $CsCuO_2$ that can be formed by a reaction of cesium with H_2O and O_2 in combination with Cu from the walls of the ion source, while the white traces were identified as cesium hydroxide CsOH. These visible deposits are an evidence for the formation of layers that are clearly much thicker than one monolayer.
However, the cesium accumulations formed on the chamber walls during source operation react within minutes after breaking the vacuum. Thus, it is difficult to draw conclusions to the chemical compositions of the deposits under vacuum without in-situ analysis.
Considering these observations, the temperature-dependent ad- and desorption of cesium on the source walls was implemented in CsFlow3D according to experimental results with a quartz microbalance measurements under ion source relevant vacuum (between

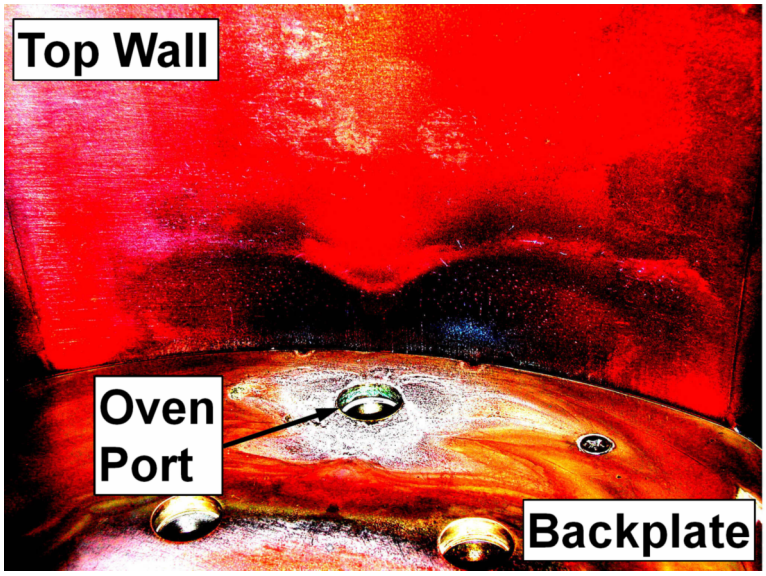

Figure 4. High contrast photograph of the backplate (molybdenum-coated) and the top wall (copper) of the ion source of MANITU after the evaporation of 1000 mg of cesium. The position of the nozzle system of the evaporation oven is located at the marked port.

10^{-3} and 10^{-4} Pa) and surface conditions [27].
The mentioned investigations showed a high surface affinity of cesium for relevant surface temperatures between 25 °C and 50 °C. While wall absorption coefficients of 0.9 and 0.7 were determined, respectively, a high cesium desorption rate and therefore negligible sticking for the investigated cesium flux was found for the temperature of the plasma grid of 150 °C is reached [27]. The corresponding high plasma grid temperature is chosen because of empirical observation giving an increase of the extracted current density in the experiment.

3.7. Thermal Desorption

Re-distribution processes of cesium within the ion source by thermal evaporation from the chamber walls determine the dynamics of cesium within the ion source predominantly. This cesium evaporation from the source walls is modeled based on a cosine distribution of the cesium velocity vector with respect to the surface normal vector. In the ion source for the MANITU test facility, the temperature is not constant for all surfaces of the ion source during plasma operation. The heat load by the plasma creates a temperature dynamics on source components which are not temperature stabilized like the bias plate. A temperature time trace from a thermo-couple within the bias plate was therefore used. The measured temperature dynamics of the bias plate during the discharge by the heat load from the impinging plasma particles was fitted and is shown in figure 5.
In summary, the wall absorption is governed by a temperature-dependent sticking factor

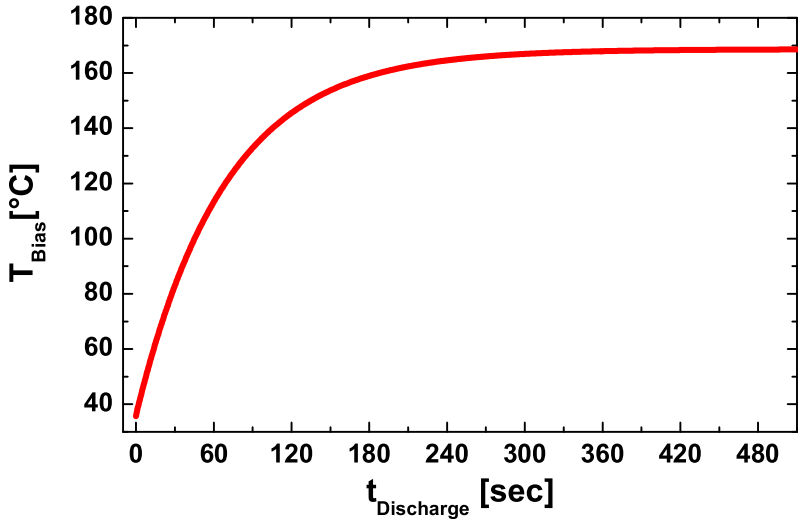

Figure 5. Dynamics of the bias plate temperature during a 500 sec H_2 pulse in MANITU.

s using the following equation:

$$\Delta\theta = \Gamma_{\mathrm{In}}\, s\, \Delta t, \tag{8}$$

where $\Delta\theta$ is the change in surface density and Γ_{In} the incoming cesium flux density for an exposure time Δt. The desorption from heated components is determined by a temperature-dependent surface flux density Γ_{Out}.

3.8. Cesium Erosion during Source Operation

Besides by thermal desorption, additional cesium sources are formed by sputtering with positive ions. Collisions of fast negative ions and fast neutralized negative ions with the residual hydrogen gas in the acceleration system generate a flux of high-energy positive hydrogen and molecular ions:

$$\mathrm{H^- + H_2 \rightarrow H^+ + 2e^- + H_2} \tag{9}$$

$$\mathrm{H^- + H_2 \rightarrow H^0 + e^- + H_2} \tag{10}$$

$$\mathrm{H^0 + H_2 \rightarrow H^+ + e^- + H_2} \tag{11}$$

$$\mathrm{H^0 + H_2 \rightarrow H^+ + 2e^- + H_2^+} \tag{12}$$

These positive ions are accelerated back into the ion source vessel in the opposite direction than the negative ions and hit the backplate of the ion source. Data of these these so called backstreaming ions for the IPP prototype source MANITU was taken from investigations presented in [29]. According to these investigations 2 % of the negative ion beam current density, which is typically 250 $\mathrm{A/m^2}$, is scattered back as $\mathrm{H^+}$ and $\mathrm{H_2^+}$ ions (0.54/0.46) having an average energy of 8 kV.
An approximate sputtering yield of 0.027 was calculated by the TRIM code [30] assuming a surface binding energy of 1 eV for the cesium layers. The latter is an estimation

of the lowest binding energy which is valid for cesium compounds with a low stability like CsH.
The flux of backstreaming ion is directed onto the backplate of the ion source vessel. However, experimental observations show areas on the sidewalls of the expansion chamber located close to the driver exit, which are totally cleaned from cesium (shiny copper surface). This significant cesium erosion cannot be explained by physical sputtering from hydrogen ions, since backstreaming ions are not capable of hitting the side wall and hydrogen ions accelerated in the sheath do not have enough energy to create significant sputtering yields.
Possible mechanisms could be thermally assisted chemical processes or physical sputtering by heavy ions such as Cs^+ (self sputtering) or Cu^+ (impurity). While the process and the corresponding desorption flux is not known, an empirical estimation of the desorption flux at the plasma exposed surfaces was used. An approximate desorption flux from the sidewalls of $4x10^{14}$ cm^{-2} sec^{-1} was assumed which reproduces the cesium erosion as observed in the experiment.

4. Results

4.1. Cesium Redistribution during the Vacuum Phase

The cesium conditions during the vacuum phases between the pulses have a high relevance, since the cesium distribution within the source after a preceding vacuum phase defines the initial conditions for the re-distribution in the subsequent operation phase.
Figure 6 shows line plots of the computed cesium accumulation rate on a) the backplate (x=120 mm) and b) the side walls (z=±144 mm, x=100 mm) of the expansion chamber for sticking coefficients between 0.1 and 0.9. The right hand side shows a logarithmic contour plot of the cesium accumulation rate at s=0.7 on the backplate of the ion source. The coefficients of 0.9 and 0.7 represent the experimentally obtained coefficients for wall temperatures of 25 °C and 50 °C, respectively. Scenarios for lower sticking coefficients were calculated in order to demonstrate the effects on the cesium distribution for changed wall conditions.
The calculation for s=0.7 shows three maxima with an accumulation rate of $5x10^{13}$ cm^{-2} s^{-1} to appear on the backplate close to the injection system (position shown in figure 1). This is an effect of the orientation and position of the nozzles of the evaporation oven pointing at the bottom- and sidewalls of the expansion chamber.
The accumulation profiles shown in figure 6 a) and b) are determined by both the profile of the injected nozzle flux and the re-distribution of cesium that is reflected from the walls. In case of a wall temperature of 25 °C, the cesium distribution within the ion source is predominantly influenced by the flow profile from the nozzle system and inhomogeneous accumulation profiles are created.

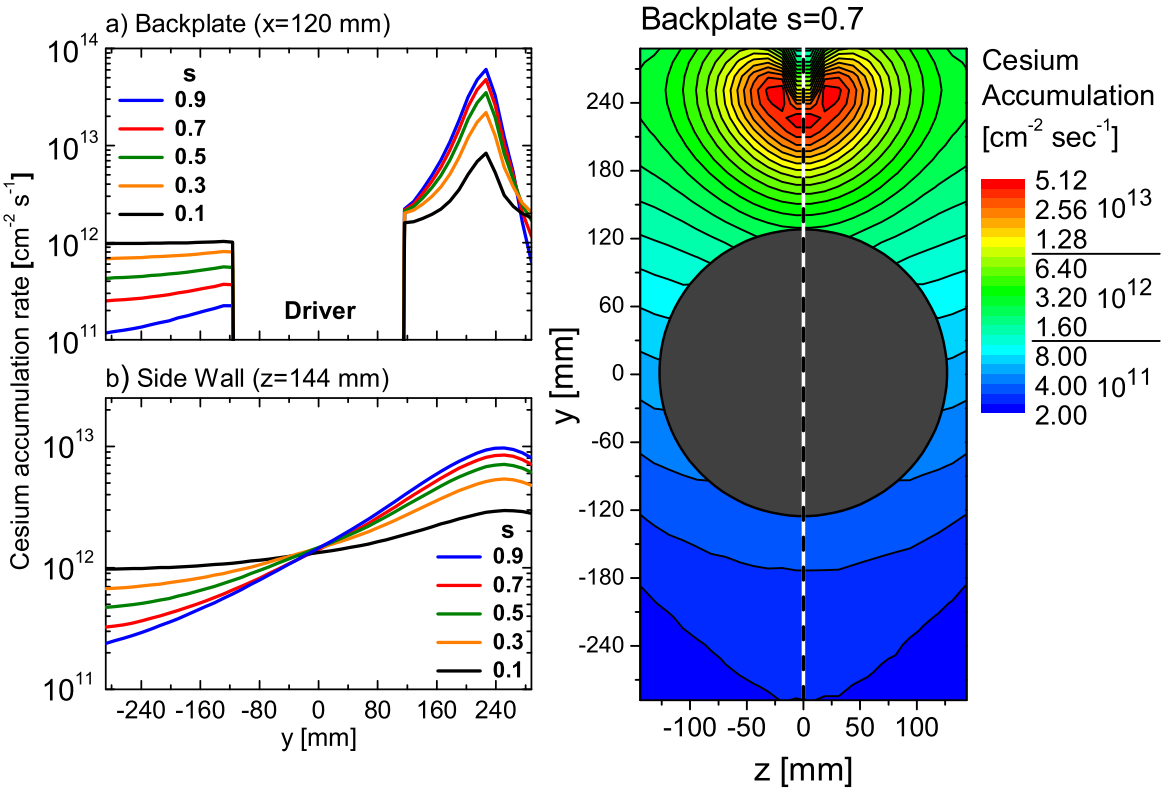

Figure 6. Computed cesium accumulation rates during a vacuum phase of the IPP prototype source of the MANITU test facility for a cesium injection rate of 10 mg/h.

Increasing the wall temperature an thus decreasing the sticking coefficients results in a better re-distribution and the cesium is more equally spread within the source chamber. Surface areas at remote locations with respect to the position of the cesium oven are supplied with cesium at the expense of the surface areas in the vicinity of the evaporation oven. This can be seen in the line plots from the decrease of the accumulation peak near the oven nozzle (y=225 mm) with lower sticking coefficients while the surface areas in the negative y-direction receive, in return, a higher cesium flux.

An area of special interest is the top wall (y=288 mm) of the ion source, since the distance of the nozzles to this wall is very short (< 3 cm) and the plasma exposure onto the top wall of the ion source is limited. Hence, the scattering force during the plasma phases will not result in a significant deviation of the corresponding wall patterns. Additionally, the vacuum phases represent the dominant operation phases of the ion source. Therefore, it is possible to compare the cesium deposits on this specific area to results from the cesium modeling of the vacuum phase. Figure 7 shows the cesium accumulation on the top wall (y=288 mm) obtained by CsFlow3D after evaporating 1000 mg of cesium for a wall temperature of 50 °C. The thickness θ of the cesium coverage was determined from the atomic radius of cesium for a monolayer coverage of

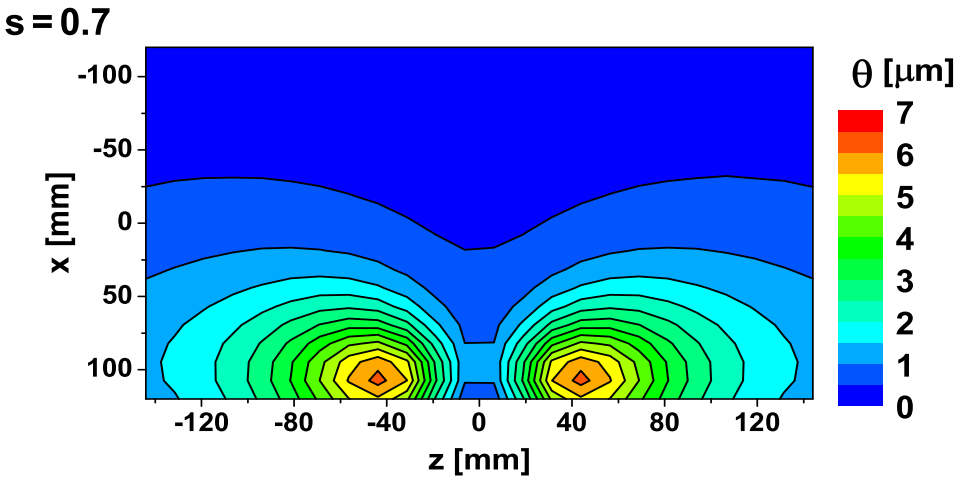

Figure 7. Computed thickness θ of the cesium layers on the top wall (y=288 mm) of the ion source of MANITU after the evaporation of 1000 mg of cesium at an influx of 10 mg/h and a wall temperature of 50°C.

$4.5\text{x}10^{14}$ cm^{-2}. Similar to the experimental observations as presented in figure 4, the computed profile shows the formation of two lobe-shaped cesium deposit structures. A maximum layer thickness of 7 μm was computed at the center of each lobe. Each lobe corresponds to one horizontal nozzle of the evaporation oven. The actual shape of the lobes is determined by the flux distribution from the nozzle and the distance to the upper wall. The presented results are in good qualitative agreement with investigation of the walls of the disassembled ion source of MANITU after the evaporation of 1000 mg as shown in figure 4 indicating that the combination of code and experimental data is capable of giving predictive results in the vacuum regime. An integration of the cesium loss through the apertures for the described case gives a considerably low amount of 25 mg after evaporating 1000 mg in total, which is a result of the high sticking coefficient of 0.7 and the direction of the nozzles on the walls of the ion source.

4.2. Cesium Dynamics during the Plasma Phase

The preceding investigations showed clearly that large quantities of cesium can be stored on the walls of the source chamber. An active recycling process of cesium from specific surface areas takes place, however, during the discharge. Cesium which is released from the chamber walls during the pulses is expected to contribute significantly to the total flux onto the plasma grid. This affects the work function and, hence, the negative ion production yield as a function of time and homogeneity.

The cesium flux onto the plasma grid was calculated for plasma pulses of several hundred seconds after a series of 100 short conditioning pulses with a length of 20 sec and preceding vacuum phases of 4 min each determining the corresponding initial condition of the cesium distribution. A source wall temperature of 50 °C and a plasma grid

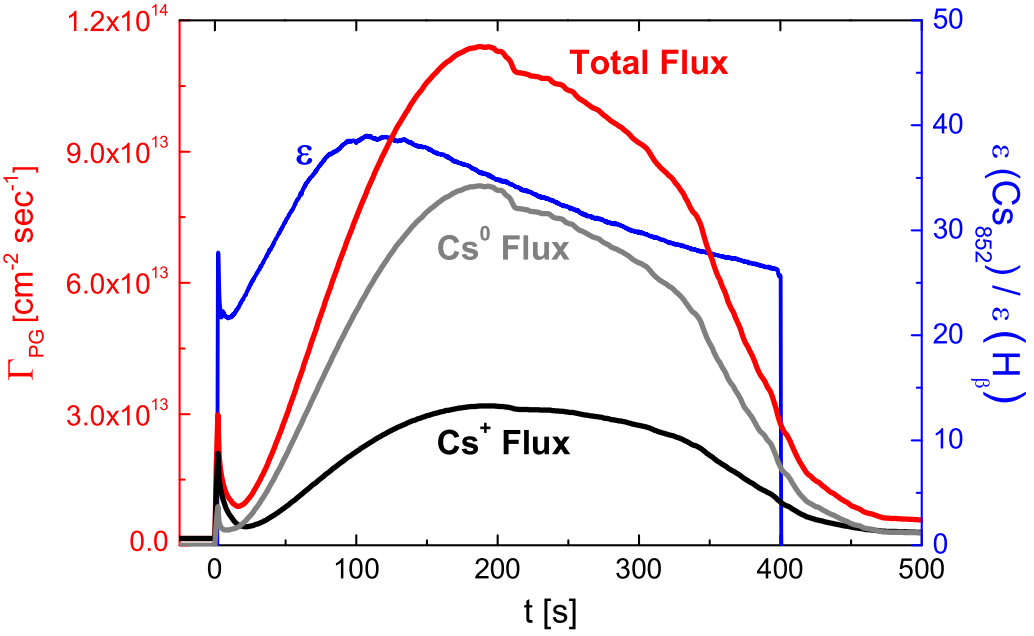

Figure 8. Computed dynamics of the integrated total, neutral and ionic cesium flux onto the plasma grid of MANITU during a plasma pulse with enabled extraction of 500 sec. Additionally, measured optical emission signal ϵ of the line ratio Cs_{852} divided by H_β during a 400 sec pulse (H_2, 0.4 Pa, 65 kW).

temperature of 150 °C was used, while the temperature time trace of the bias plate was used according to figure 5. According to this duty cycle, an average cesium layer thickness within the range of 10^{16} cm^{-2} is created on the bias plate. The mentioned conditioning scenario was chosen since optimized duty cycles are necessary at the ion source test facility to obtain the full performance of the ion source [13][31].

Figure 8 shows the computed time trace of the ionic and neutral cesium flux (j_{Cs^+} and j_{Cs^0}) onto the plasma grid and the apertures for a pulse length of 500 sec and the specified conditioning scenario. In the simulation this is approximately the time length until a significant decrease of the flux takes place. In order to compare the simulated cesium flux with experimental data, a time trace of the optical emission spectroscopy (OES) signal for the neutral cesium line at 852 nm for a line-of-sight close to the plasma grid is also shown in parallel to the simulation data. The OES signal is proportional to the density of neutral cesium in front of the plasma grid $\epsilon \propto n_{Cs_0} n_e$ and, hence, to the corresponding cesium flux density. A normalization by the H_β OES signal was done in order to reduce the influence of changes of the electron density during the discharge. The intensity of optical emission from cesium ions is too low in order to give a significant signal.

Both, the simulation and the OES signal show a high dynamic of the cesium re-distribution. An initial peak of the cesium flux onto the plasma grid within the range of 3x10^{13} cm^{-2} s^{-1} appears in the first seconds of the discharge. The simulation shows

that this flux consists primarily (>70%) of cesium ions.
Backtracing the particle trajectories reveals that the initial peak originates from both, the release of cesium by from the side walls close to the driver and the backstreaming ions with cesium reservoirs at walls near the driver exit and on the backplate. The released reservoirs were accumulated during the preceding vacuum phases and short plasma pulses. An explanation for the high content of ions during the initial peak is given by the high electron density and temperature near to desorption surfaces. For example, at a typical electron temperature of $T_e \approx 8$ eV and density of $n_e \approx 10^{18}$ m^{-3} in the expansion region (see figure 2), the mean free path length for ionization of atomic cesium at a temperature of 1200 K is less than 0.5 cm.
The initial peak of the flux decays after 20 sec which is a consequence of the depletion of the reservoirs that were formed during the vacuum phase. After the decay of the initial peak, a second, more intense peak appears both, in the simulation and the OES. According to the simulation, this peak is dominated by neutral cesium and, hence, the cesium spectroscopy is expected to have a high sensitivity. The simulation shows that thermal desorption from the bias plate, heated by the plasma during the long pulse, creates the dominant contribution to this peak. Due to the low electron temperature below 2 eV and density of several 10^{17} m^{-3} in the vicinity of the bias plate, the mean free path length for ionization close to the bias plate is within the order of several tens of centimeters. As a consequence, the time trace of cesium onto the plasma grid, released from the bias plate, is dominated by neutral cesium.
The comparison of the prediction from CsFlow3D with the OES time trace of atomic cesium indicates a good qualitative agreement. Nevertheless, the actual decay time of the OES signal is longer than in the simulation. This is probably an effect of different initial conditions of the cesium deposits in the ion source. The initial accumulation of cesium on the bias plate before a plasma pulse is influenced by the history of cesium injection and removal during the preceding operation time of the ion source and, hence, the complete temperature history of the bias plate itself during the preceding source operation phases. Therefore, an improved temperature control in combination with a modeling of the transient temperature distribution will be the first step to improve the time stability of the cesium distribution within the ion source.

4.3. Cesium Flux Distribution onto the Plasma Grid

As a consequence of the large dimensions of the extraction system for ion sources for N-NBI, the homogeneity of the flux profile onto the plasma grid plays an important role besides the time dynamics. Vertical profiles (±y-direction, z=0 mm) of the calculated cesium flux onto the plasma grid during the vacuum phase and at different times during plasma operation (corresponding to figure 8) are shown in figure 9. Figure 9 a) shows that a cesium flux within the range of 10^{12} cm^{-2} s^{-1} is obtained during the vacuum phases. The calculated flux within the initial peak (see figure 9 b)) and the second peak of the operation phase (see figure 9 c)) is by a factor of 10 and 100 higher, respectively.

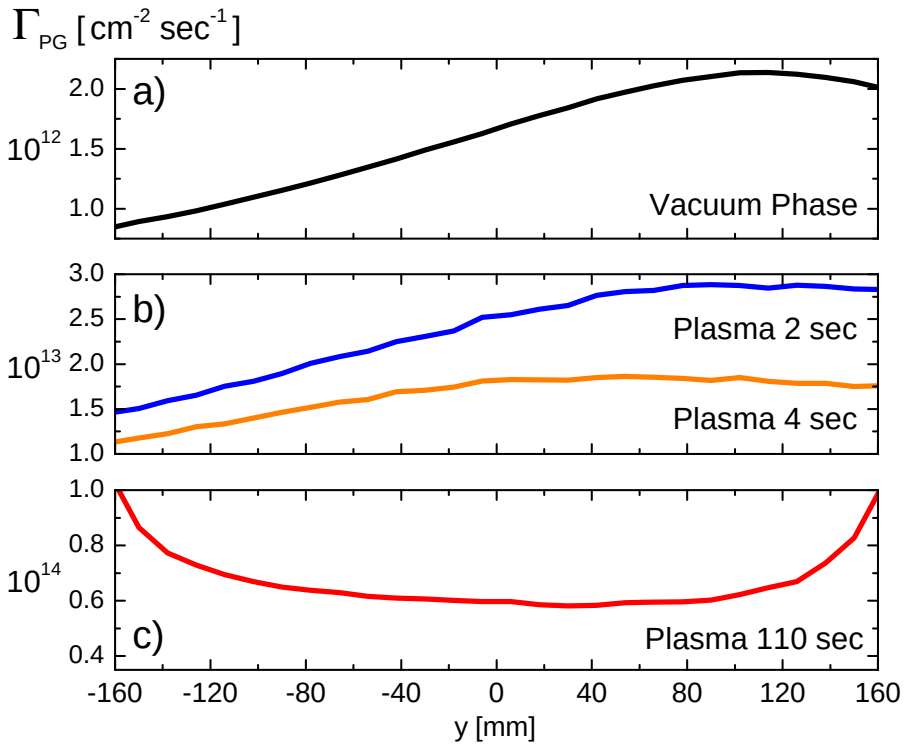

Figure 9. Computed vertical profiles of the total cesium flux density onto the plasma grid Γ_{PG} during a) the vacuum phase and at different times of the operation phase of the ion source (curves b) and c)) for a cesium injection rate of 10 mg/h.

As a consequence of the low cesium flux during the vacuum phase, it will take several minutes to replenish a single monolayer of cesium during the vacuum phase, while in the discharge phase, this process takes place in several seconds.

Figure 9 a) and b) show an inhomogeneity regarding the cesium flux onto the upper area of the plasma grid, which is by a factor two more intense than the one onto the lower area. In both cases this effect is caused by the position of the nozzle system at the upper part of the source (+y-direction). The upper area of the plasma grid is illuminated better by the nozzles of the oven and by cesium that is thermally re-distributed from the chamber walls. This explains the described effect in the vacuum phase.

As explained in the previous section, the cesium flux on the plasma grid during the first seconds of source operation is determined by the cesium distribution of the preceding vacuum phase. An inhomogeneous distribution of cesium deposits is formed in this vacuum phase - a direct consequence of the position of the cesium nozzle and its high surface affinity.

A different flux profile was obtained after long pulse times. Figure 9 c) shows the cesium flux profile at a time of 110 sec during the increase of the second peak shown in figure 8. As mentioned before, this peak is created by thermal desorption of cesium from the bias plate. Corresponding to the geometry of the bias plate, a more intense cesium flux

was computed close to the bias plate areas where the thermal desorption process takes place. Additionally, a profile with top/down symmetry (positive/negative y-axis) can be observed within the first 100 sec of the second peak, since equivalent desorption rates of the cesium deposits on the upper and lower part of the bias plate are obtained.
As a consequence of the lower amount of cesium in the lower (-y-direction) part of the source, these deposits are depleted at first and the total flux is reduced. This explains the presence of a finite decay time of the second peak in figure 8.

5. Conclusion and Outlook

The 3D Monte Carlo based test particle code CsFlow3D was developed and applied to simulate the dynamics of neutral and ionic cesium during the vacuum and the plasma phases of the IPP RF-driven negative-ion source used for the MANITU test facility. CsFlow3D is capable of computing the dynamics and homogeneity of the cesium re-distribution within the ion source. A successful validation of the simulation during the vacuum phase was accomplished by a comparison to the cesium accumulation traces after breaking the vacuum. The comparison of the code results during the plasma phase with the OES signal of neutral cesium shows a good agreement with the corresponding temporal variation.
The simulation of the cesium re-distribution during the vacuum phase for different wall temperatures showed the formation of cesium deposits especially on the surface area close to the cesium oven. Increasing the wall temperature from 20°C to 50°C turned out to generate a more even distribution within the ion source chamber at the expense of cesium on remote surface areas with little contact with the plasma. This is beneficial for the recovery of cesium from the deposits and, therefore, for the cesium flux onto the plasma grid. The simulation of the time dynamics of the total cesium flux onto the plasma grid demonstrated that the formation and depletion of cesium reservoirs on the walls, formed during the preceding source operation, is the dominant factor for the cesium flux onto the plasma grid.
Besides the impact on the time dynamics, the release of cesium reservoirs during the discharge turned out to have also large influence on the intensity and profile of the cesium flux onto the plasma grid. As a consequence of the release of reservoirs, the cesium flux during the discharge is up to a 100 times larger than during the vacuum phase. Inhomogeneous flux profiles during vacuum and plasma phases were computed as a direct consequence of the initial distribution and the position of the cesium nozzles. These flux inhomogeneities will affect the negative ion production, since experimental investigations of the reflected cesium flux from a hot metal surface under relevant conditions [27] show very high thermal evaporation rates making it impossible to grow large deposits of clean cesium on the converter surface for the calculated fluxes.
In summary, the presented investigations show that no immediate control and, hence, regulation of the cesium flux onto the plasma grid is possible by changing the cesium injection rate of the supply. The instable depletion of cesium reservoirs and

an inhomogeneous flux profile needs to be avoided and constant and homogenously distributed cesium flux is desirable. The development of a cesium flux control system in order to stabilize the extracted ion and electron current is required in order to fulfill the ITER criteria.
An improved control of the formation and release of reservoirs in combination with an optimized cesium injection is therefore required. This can be done by external heating and plasma exposure of surface areas with high cesium accumulation and by an improved temperature stability of the bias plate. Additionally, a cesium injection system in the extraction region close to the plasma grid is a promising approach to improve the time stability of the cesium flux.
Simulations to obtain an optimized cesium injection with respect of stability and homogeneity by the use of an array of cesium dispensers close to the plasma grid will be presented soon.

Acknowledgments

This work was (partly) supported by a grant of F4E (Fusion For Energy). The authors are solely responsible for the content.

References

[1] R. S. Hemsworth, A. Tanga and V. Antoni, *Rev. Sci. Inst.* **79** (2008), 02C109
[2] K.H. Berkner, R. V. Pyle and J. W. Stearns, *Nucl. Fus.* **15** (1975), 249
[3] ITER Technical Basis 2002, ITER EDA Documentation Series No 24 (Plant Description Document, section 2.5.1), IAEA Vienna
[4] E. Speth, H. Falter, P. Franzen, U. Fantz et al, *Nucl. Fusion* **46** (2006), 220
[5] M. Bacal, E. Nicolopoulou, and H. Douset, Proc. Int. Symp. Production and Neutralization of Negative Ions and Beams, 26 (New York), BNL, 1977
[6] Y. Belchenko, G. Dimov, and V. Dudinikov, *Nucl. Fusion* 14 (1974), 113
[7] P. W. Van Amersfoort, J. J. C. Geerlings, L. F. Tz. Kwakman, et al., *J. Appl. Phys.* 58 (1985), 3566.
[8] W. G. Graham, Proceeedings of the Second International Symposium on the Production and Neutralization of Negative Hydrorgen Ions and Beams, Brookhaven National Laboratory, Upton, 1980, p. 126.
[9] R. Gutser, C. Wimmer, and U. Fantz, *Rev. Sci. Instrum.* 82 (2011), 023506.
[10] A. Tanga, M. Bandyopadhyay, and P. McNeely, *Appl. Phys. Lett.* 84 (2004), 182.
[11] U. Fantz et al, *Nucl. Fusion* **46** (2006), S297
[12] W. Kraus et al., *AIP Conf. Proc.* 1097 (2009), 275
[13] W. Kraus et al., *Rev. Sci. Inst.* **79** (2008), 02C108
[14] Yu. I. Belchenko, G. I. Dimov, and V. G. Dudnikov, Brookhaven National Laboratory Report No. BNL 50727 79, 1977.
[15] R. Gutser, D. Wünderlich, and U. Fantz, *Plasma Phys. Control. Fusion* 51 (2009), 045005
[16] A. Kirschner, V. Philipps, J. Winter, et al., *Nucl. Fusion* 40 (2000), 989
[17] M. Lukomski, S. Sutton, W. Kedzierski, et al., *Phys. Rev. A* 74 (2006), 032708
[18] H. Hutchinson, Principles of plasma diagnostics, Cambridge University Press, Cambridge UK, 2002

[19] D. Lide, CRC Handbook of Chemistry and Physics, 88th Edition (CRC Handbook of Chemistry and Physics), CRC, 2007
[20] J.D. Huba, NRL plasma formulary, Naval Research Laboratory, 2006
[21] E. Rothe and R. Bernstein, *J. Chem. Phys.* 31 (1959), 1619
[22] S. Ma, R. Sydora and J. Dawson, *Comp. Phys. Comm.* **77** (1993), 190
[23] C. Birdsall, *IEEE Trans. on Plasma Sci.* **19**, 1991, 65
[24] B. Crowley and S. Dietrich, *Plasma Sources Sci. Technol.* 18 (2009), no. 1, 014010
[25] P. McNeely, S. Dudin, S. Christ-Koch, et al., *Plasma Sources Sci. Technol.* 18 (2009), 014011.
[26] D. Ciric, Private communication, 2006, JET Joint Undertaking, Abingdon
[27] U. Fantz, R. Gutser and C. Wimmer, *Rev. Sci. Instrum.* 81, 1 (2010)
[28] G. A. Bird, Molecular gas dynamics and the direct simulation of gas flows, Clarendon Press, Oxford, 1994.
[29] L. Schiesko, Sputtering yield in MANITU, Tech. report, Max-Planck-Institut für Plasmaphysik, Technology Division, 2009.
[30] W. Eckstein et al, *Appl. Phys.* **A38** (1985), 123
[31] W. Kraus, U. Fantz and P. Franzen, *Rev. Sci. Inst.* **81** (2010), 02B110